Hindawi
Advances in Polymer Technology
Volume 2021, Article ID 3596591, 10 pages
https://doi.org/10.1155/2021/3596591

Research Article

Effect of Sepiolite-Loaded Fe_2O_3 on Flame Retardancy of Waterborne Polyurethane

Tong Xu,[1] **Di Qian**,[1] **Yelei Hu**,[1] **Yuanzhao Zhu**,[1] **Yi Zhong**,[1] **Linping Zhang**,[1,2] **Hong Xu**,[1] **Huaxin Peng**,[3] **and Zhiping Mao**[1,4,5]

[1]*Key Laboratory of Science & Technology of Eco-Textile, Ministry of Education, Donghua University, Shanghai 201620, China*
[2]*Tsinghua Univ, Dept Chem, Minist Educ, Key Lab Bioorgan Phosphorus Chem & Chem Biol, Beijing 100084, China*
[3]*Zhejiang University, Institute for Composites Science Innovation, Hangzhou, Zhejiang Province, 310058, China*
[4]*National Dyeing and Finishing Engineering Technology Research Center, Donghua University, No. 2999, North Renmin Road, Songjiang District, Shanghai 201620, China*
[5]*National Manufacturing Innovation Center of Advanced Dyeing and Finishing Technology, Taian, Shandong Province 271000, China*

Correspondence should be addressed to Hong Xu; hxu@dhu.edu.cn and Zhiping Mao; zhpmao@dhu.edu.cn

Received 14 September 2021; Revised 26 October 2021; Accepted 9 November 2021; Published 25 November 2021

Academic Editor: Pierre Verge

In this study, a kind of inorganic composite flame retardant (Sep@Fe_2O_3) was prepared by combining solution deposition and calcination methods using sepiolite microfiber material as carrier. This inorganic compound flame retardant was combined with waterborne polyurethane (WPU) through layer-by-layer method to prepare WPU composites. The SEM and EDS, TEM, and XRD were used to characterize the microscopic morphology and crystal structure of WPU composites. Thermogravimetric analysis tests confirmed the good thermal stability of WPU/Sep@Fe_2O_3 composites; at the temperature of 600°C, the carbon residual percentage of WPU/Sep, WPU/Fe_2O_3, and WPU/Sep@Fe_2O_3 composites is 7.3%, 12.2%, and 13.4%, respectively, higher than that of WPU (1.4%). Vertical combustion tests proved better flame-retardant property of WPU/Sep@Fe_2O_3 composite-coated cotton than noncoated cotton. The microcalorimeter test proved that the PHRR of WPU/Sep@Fe_2O_3 composites decreased by 61% compared with that of WPU. In addition, after combining with Sep@Fe_2O_3, the breaking strength of WPU increased by 35%.

1. Introduction

As an eco-environmentally polymer material that could replace traditional solvent-based polyurethane, waterborne polyurethane (WPU) has been used more and more widely in producing apparel, clothing, home furnishings, and industrial products in recent years [1, 2]. However, the flammability and poor heat resistance of WPU are a huge obstacle to its application in firefighter's protective clothing and military and airline industry [3]. Previous research on flame retardant polyurethane has mainly focused on solvent-based polyurethane (PU) [4, 5]. For example, Chen et al. studied on thermal properties of PU nanocomposites based on organic sepiolite [6], but the thermal stability of PU composites is not as good as expect. Zheng et al. researched the characterization of sepiolite/PU nanocomposites [7]; the TG results of sepiolite/PU nanocomposites identified slightly improved. Due to the different dispersion systems of WPU and PU, their molecular structures and properties are also different, leading to the requirements for flame-retardant property also being different. The current situation is that there are a few of studies on the flame-retardant property mainly for WPU. Han et al., Kim et al., and Yeh et al. studied the flame-retardant property of WPU/clay composites; the flame-resistant property of these materials could only be improved a little [8–10].

As society is progressing, human beings become more aware of environmental protection. Even though many

conventional flame retardants exhibit excellent flame resistance, halogen-containing flame retardants are banned due to serious environmental problems. Phosphorus- and nitrogen-containing flame retardants as the second category of optional flame retardants still have some environmental problems, such as eutrophication of water caused by the discharge of phosphorus-containing wastewater into the natural world [11–21]. Therefore, there is an urgent need for an environmentally friendly, efficient, and convenient flame retardant.

The researchers proposed that sepiolite- (Sep-) loaded metal oxides could be used for preparing flame-retardant polymer. Sep as a natural silicate material, which is not combustible itself, is nonpolluting to the environment and nonhazardous to human beings. However, when the material is used as flame retardant alone, the flame retardancy is not excellent [22–24]. For these reasons, an inorganic composite flame retardant is prepared by loading the transition metal oxide which has Lewis's acid property and could act as a kind of catalytic carbon formation agent on Sep. Therefore, this inorganic composite flame retardant could enhance the flame-retardant property of polymer by improving the carbon formation of the substrates. For example, Guillon prepared a series of catalyst which comprised at least one IZM-2 zeolite, one matrix, and one metal selected from metals of groups VIII, VIB, and VIIB. Those catalysts promote rapid thermal decomposition of polymers to generate carbonization [25]. Aranda et al. prepared layered double hydroxide/Sep heterostructured materials and investigated the catalytic properties of the above materials [26]. Yuming Chen and Limin Zhou studied energetics and mechanisms of graphene growth catalyzed by nickel nanoclusters by using ab initio density functional theory calculations [27].

These previous works made believed that loading transition metal oxides into Sep could enhance the carbon-forming effect of Sep. However, what will happen if transition metal oxide is combined with Sep to form a flame-resistant system for WPU? In this study, inorganic composites (Sep@Fe_2O_3) were prepared by combining precipitation and calcination methods to load Fe_2O_3 into Sep crystals; organic/inorganic composites were prepared by combining these inorganic composites with WPU by layer-by-layer (LBL) method to study the thermal stability and combustion properties of these composites and explore the mechanism of the effect of Sep@Fe_2O_3 on the combustion property of WPU.

2. Experimental

2.1. Materials. Sep was obtained from Zhejiang Fenghong Chemical Co., Ltd., China. Both Fe $(NO_3)_3{\cdot}9H_2O$ (AR) and NaOH (AR) were purchased from Sinopharm Chemical Reagent Co., Ltd., China. WPU (SR-5428) was purchased from Sitoke New Material Co., Ltd., China.

2.2. Preparation of Sep@Fe_2O_3. In this work, Sep@Fe_2O_3 precursor was prepared by dispersing the Sep fiber in deionized water/ethanol (1/1) at 25°C, followed by adding 100 mL Fe $(NO_3)_3$ solution (0.05 mol/L) with stirring under nitrogen atmosphere for 45 min. In this system, the amount of iron ions is double the cation exchange capacity (CEC) of Sep (93.7 mmol/100 g). Then, 100 mL NaOH solution (0.11 mol/L) was added to the solution with high-speed stirring for 2 h. The slurry aged in the darkroom for 20 min and then was separated by centrifugation (TG20G, Spring Instrument. Co., Ltd., China), washed by deionized water, and dried at 105°C for 4 h. The prepared dry chips were calcinated in muffle furnace (GST-3-1200-I, Shanghai Guangshu Electromechanical Co., Ltd.) at 400°C for 4 h to prepare Sep@Fe_2O_3 composite material.

2.3. Preparation of WPU/Sep@Fe_2O_3 Composites. All films were assembled on a given substrate using the procedure shown in Figure 1. Each substrate was dipped into the deposition mixtures, alternating between the WPU emulsion of 3.0 wt.% and inorganic materials (Sep, Fe_2O_3, and Sep@-Fe_2O_3) of 0.2 wt.%, with each cycle corresponding to one bilayer (BL). Each dip was followed by handling with a stream of filtered air for 60 s, the above process was repeated for 10 times, and then WPU composites were prepared. Samples of WPU composites are shown in Table 1.

2.4. Characterization. The microstructure characterization of Sep samples and WPU composites was carried out by X-ray diffractometer (XRD, 6100), transmission electron microscope (TEM, SU-70t), and scanning electron microscopy (SEM, SU-3500). The XRD spectrum of synthesized catalysts was obtained by radiation Cu Ka ($\lambda = 1.54$ Å). Samples of TEM were embedded in 812 resin (TAAB, UK), and ultrathin sections (about 800 nm thick) were cut on a Leica ultramicrotome (Leica Microsystems, Milton Keynes, UK sections) viewed in a SU-70t TEM. The election high tension (EHT) of SEM was set at 10 kV, and imaging was carried out using SE2 detector. Due to the nonconductive nature of the WPU composites, the samples were sputter-coated with a thin layer of gold prior to the imaging using a Polaron SC 7640 for 60 s. ATR-FTIR spectrophotometry was used to determine the surface structure of the WPU composites and to qualitatively determine the presence of the organic modifiers in the WPU composites. A Tensor 27 model infrared spectrophotometry with attenuated total reflectance module with monolithic diamond crystal for full spectral range from 4000 to 400 cm^{-1} was used.

The thermal stability of samples was measured in a thermal gravimetric analyzer (TG, SDT Q600). Each sample was approximately 5 mg and tested from 30°C to 900°C at a heating rate of 20 mL min^{-1}. The vertical flame test (VFT) was performed according to BG/T 5455-1997, by using a vertical burning tester (BCR-A, Textile Science Institute, Shandong, China). The samples (300 mm × 80 mm) were prepared using the procedure shown in Figure 1. The above-mentioned substrate for preparing the WPU composite film was changed into cotton textile (115 g/m^2, Zhuocheng Special Textile Co. Ltd., Xinxiang, China), and we could get cotton-WPU composite materials. Then, the samples held 19 mm over the Bunsen burner were first exposed to the flame for a period of 12 s and then removed rapidly, the test was repeated three times for each sample, and after which,

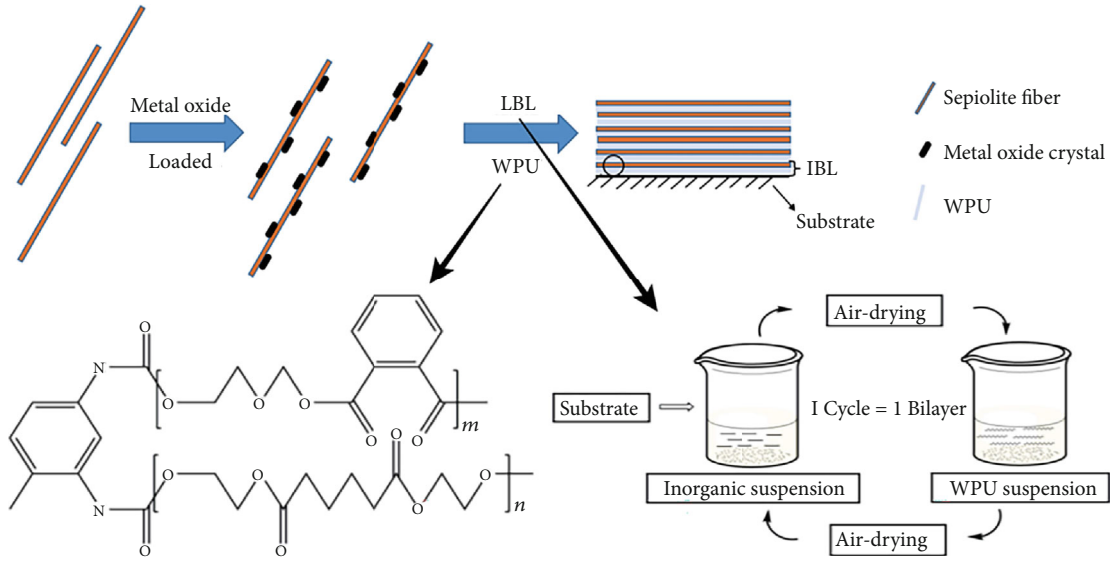

Figure 1: Schematic of WPU composite preparation.

Table 1: Sample number of film samples.

Sample number	Sample composition	Weight percentage of inorganic composites (wt.%)
S-1	WPU	0.0
S-2	WPU/Sep	6.7
S-3	WPU/Fe_2O_3	6.7
S-4	WPU/ Sep@Fe_2O_3	6.7

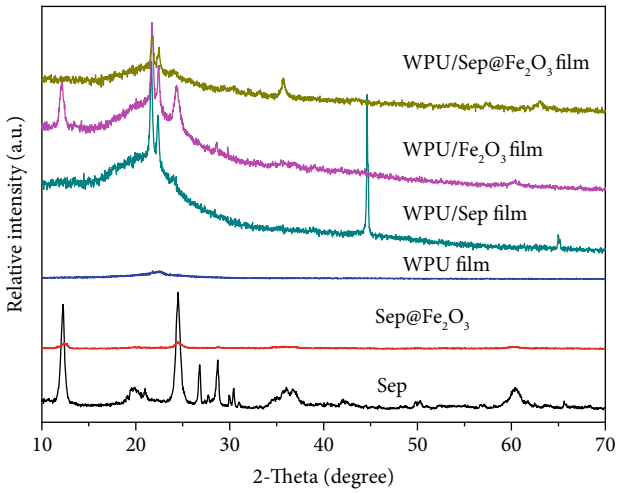

Figure 2: XRD curve of Sep samples and WPU composite films.

the after-flame and after-glow times were read from the VFT machine.

The combustion performance of samples was determined by a Microscale Combustion Calorimeter (MCC, MCC-2, Govmark, USA) instrument equipped with a 40 μL alumina pan. The samples (~5 mg) were first heated from room temperature to 750°C in an 80 cm^3/min nitrogen stream flowing at a linear heating rate of 1°C. Then, the gaseous pyrolysate mixture was mixed with a 20 cm^3/min oxygen stream flow and combustion in a furnace at 900°C for 10 s.

Tensile tests of WPU composites were carried out according to standard GB/T 1040.3-2006 on UTM 6203 machine (Shenzhen Sansi Vertical and Horizontal Technology Co., Ltd., China), and the test was repeated 3 times for each sample.

3. Result and Discussion

3.1. Structure Characterization of Samples

3.1.1. Crystal Structure of Samples: XRD Analysis. The results of the XRD test are shown in Figure 2. In the XRD patterns of the Sep and Sep@Fe_2O_3 composites, the characteristic peaks of Sep were weak in the Sep@Fe_2O_3 composites, indicating that the addition of Fe_2O_3 in the Sep@Fe_2O_3 composites affects the reading of the characteristic peak data of Sep [28]. The peak positions of Sep@Fe_2O_3 composites show good agreement to the standard data of Fe_2O_3 structure (PDF: 85-0987, 24.20° represents the characteristic peak of the 110 crystal plane, 35.73° represents that of -110 crystal plane). We observe reflexes associated with the (110) and (-110) planes; the intensity of the (110 crystal plane) reflexes is the highest. This suggests the successful preparation of Sep@Fe_2O_3 composites. In addition, no characteristic peak of other materials is found in XRD patterns, suggesting that the material is the composites of Sep with Fe_2O_3.

The results of crystal characterization of WPU film and WPU/Sep@Fe_2O_3 film are shown in Figure 2. XRD diffraction pattern of WPU film shows a broader diffraction peak, indicating that the WPU film is semicrystalline in nature. The peak at about 22.56°, which is the characteristic peak of WPU, corresponds to the (110) plane of WPU representing scattering from WPU chains at interplanar spacing

Element	Weight percentage (%)	Atomic percentage (%)
C K	4.66	7.35
O K	51.75	61.29
Mg K	20.94	16.32
Al K	0.27	0.19
Si K	21.62	14.59
Fe K	0.76	0.26
Total amount	100.00	100.00

(a)

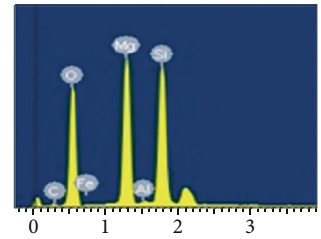

(b)

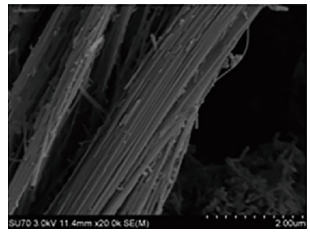

(c)

Element	Weight percentage (%)	Atomic percentage (%)
C K	17.20	24.42
O K	53.27	56.78
Mg K	15.07	10.57
Al K	0.40	0.25
Si K	12.24	7.43
Fe K	1.82	0.55
Total amount	100.00	100.00

(d)

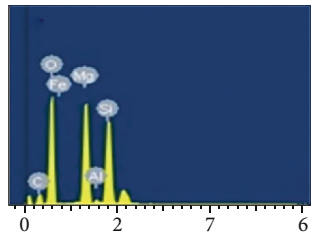

(e)

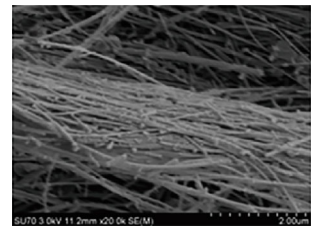

(f)

Figure 3: SEM and EDS: (a, b) EDS of Sep, (c) SEM of Sep, (d, e) EDS of Sep@Fe_2O_3, and (f) SEM of Sep@Fe_2O_3.

[29–31]. In addition, the XRD of pure WPU shows the low crystallinity of the sample which is due to repetition of benzenoid rings [32].

The XRD pattern of the WPU/Fe_2O_3 membrane shows peaks at 24.20°, 35.73°, and 62.60°, confirming the presence of Fe_2O_3 nanoparticle within the membrane, indicating the successful incorporation of Fe_2O_3 nanoparticles into the polymer matrix. The XRD pattern of the WPU/Sep@Fe_2O_3 membrane shows the characteristic peaks at 21.67°, 22.42°, 30.73°, and 35.22°, representing the crystalline nature of Sep (PDF: 75-1597). The XRD pattern of the WPU/Sep membrane confirms the presence of Sep within the membrane. The characteristic peaks of Sep are weaker obviously in the WPU/Sep@Fe_2O_3 composites, indicating that the addition of WPU and Fe_2O_3 in the WPU/Sep@Fe_2O_3 composites affects the reading of the characteristic peak data of Sep in XRD.

For WPU compounding with different kinds of inorganic materials, a shift to the right of the crystalline peaks at 21.67° and 22.42° (to 21.80° and 22.48°) is observed. The increase in intensity of the crystalline peaks of WPU composites is attributed to the enhancement of the crystallization portion in the composites caused by the addition of Sep and Fe_2O_3. This indicates that inorganic materials could promote WPU crystallization. The shift in diffraction peak is due to the change in interlayer volume caused by the insertion of inorganic materials into WPU. The increase in crystallinity of WPU composites is due to the intermolecular interaction between the polar groups of iron oxide particles and Sep with the polar group of WPU, which leads to an ordered structure in the polymer matrix.

3.1.2. Surface Morphology and Elemental Analysis of Samples with SEM and EDS. SEM images and EDS analysis data of Sep microfibers and Sep@Fe_2O_3 composites are shown in Figure 3. It can be seen from SEM images of Sep that the Sep microfibers presented in the form of dispersive fibers with a high length-diameter ratio, and there is a distinct difference between Sep and Sep@Fe_2O_3 composites which can be illustrated from the particles covered on the surfaces of Sep microfibers. Combined with EDS data, we could believe that the particles on the Sep are Fe_2O_3 crystals, proving the successful loading of Fe_2O_3 crystals on Sep microfibers.

EDS data of Sep and Sep@Fe_2O_3 composites shows the relative element content of Si, O, Mg, Al, and Fe. The weight percentage of Fe element in Sep@Fe_2O_3 composites is almost 139.5% higher than that in Sep, which also confirms the result that Fe_2O_3 is loaded in Sep microfibers successfully.

3.1.3. Internal Structure of Samples: TEM Studies. Sep structure is shown in Figure 4(a); the nature and location of metallic species within the Sep structure are shown in Figures 4(b) and 4(c). There are several approaches that Fe^{3+} interacts with Sep, which had been purified by HCl in this work. The research has proved that the purified treatment of Sep ore could remove enough Mg^{2+} cations from

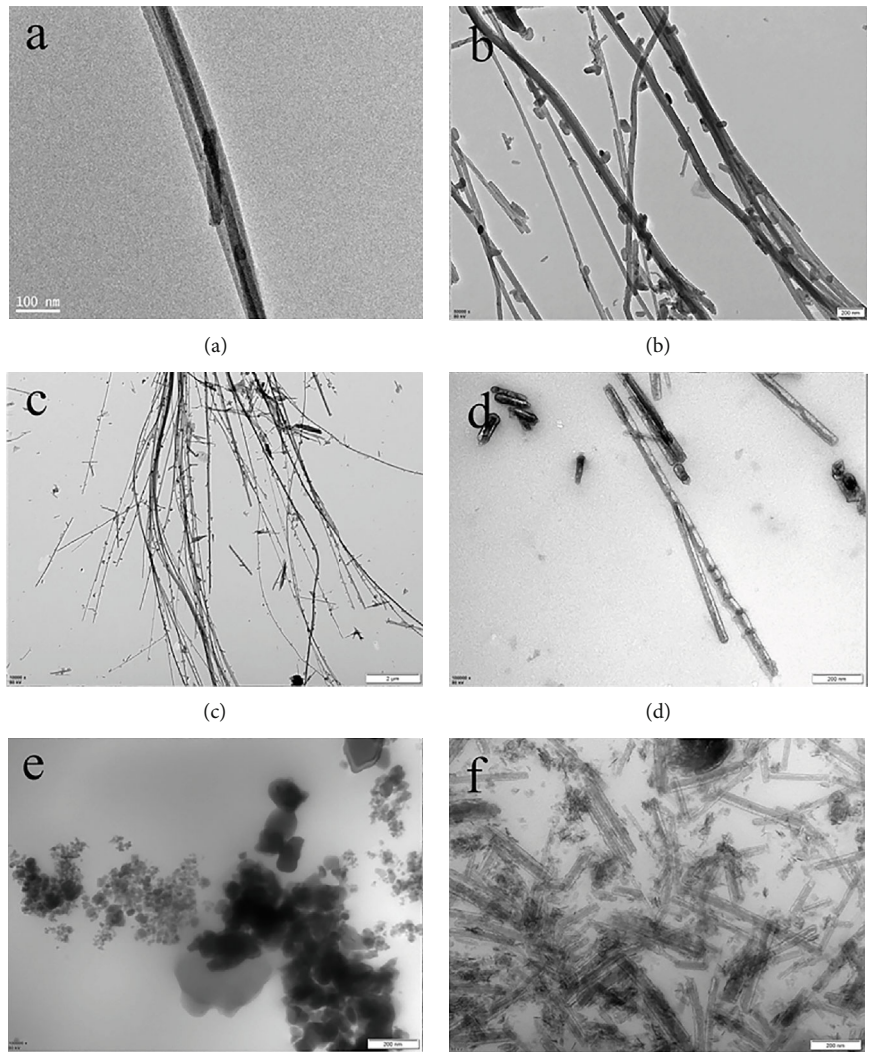

Figure 4: TEM of samples: (a) Sep, (b, c) Sep@Fe_2O_3, (d) WPU/Sep, (e) WPU/Fe_2O_3, and (f) WPU/Sep@Fe_2O_3.

Sep framework, and then, the Sep could convert to porous silica [33]. In this research, part of Fe^{3+} is incorporated into the magnesium vacancies of Sep to form variety of stable metallic-containing Sep [34, 35]. Once all the magnesium vacancies have been occupied and in case the aqueous solution contains an excess of Fe^{3+}, which would precipitate on the Sep surface as crystallized Fe_2O_3 or Fe $(OH)_3$, this is the case of metal ion interacting via electrostatic attraction. The Sep microfiber is an anionic clay mineral that offers binding sites to immobilize the positively charged particles through electrostatic interactions. In addition, from the TEM image (Figure 4(b)), we could analyze that the diameter of Fe_2O_3 is about 25-70 nm by ImageJ (shown in Figure 5(a)).

TEM image analysis can be used to quantify the distribution of Sep fiber lengths and observe the interface of substances with different properties. WPU composite membranes are analyzed by TEM and shown in Figures 4(d)–4(f). In the TEM images of WPU/Sep composite membranes (Figure 4(d)), the Sep fiber bundles completely strip in nanoscale and disperse evenly in the WPU matrix. The TEM image of WPU/Fe_2O_3 membrane (Figure 4(e)) shows that the particle size of Fe_2O_3 crystal is not uniform (shown in nanoscale and micron scale, Figure 5(b)). In addition, there is no obvious phase interface between Fe_2O_3 crystal and WPU matrix. This could prove that the compatibility of organic and inorganic phases is very excellent. TEM of WPU/Sep@Fe_2O_3 composite membrane is shown in Figure 4(f), in which the Fe_2O_3 crystal loaded abundantly on the surface of Sep fibers, which dispersed in the WPU matrix. No phase interface could be found between the interface of Sep and WPU matrix; it means that the two phases (organic and inorganic phases) are compatible. This is manifested in the greater improvement in mechanical and thermal properties which would be discussed in the subsequent sections.

3.2. Properties of Nanocomposites

3.2.1. Thermal Property of Samples: TG. As mentioned in Introduction, we believe that Sep and Fe_2O_3 can be used as

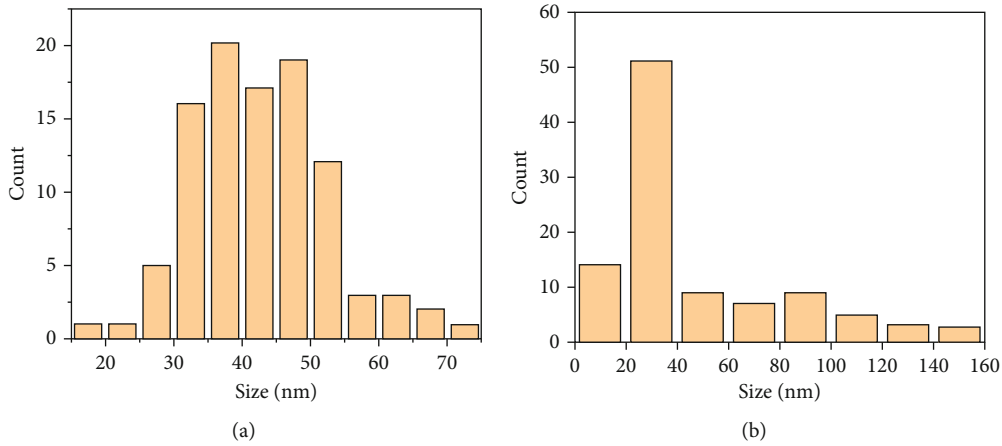

Figure 5: The diameter of Fe_2O_3 (a) from Figure 4(b) and (b) from Figure 4(e), analyzed by ImageJ.

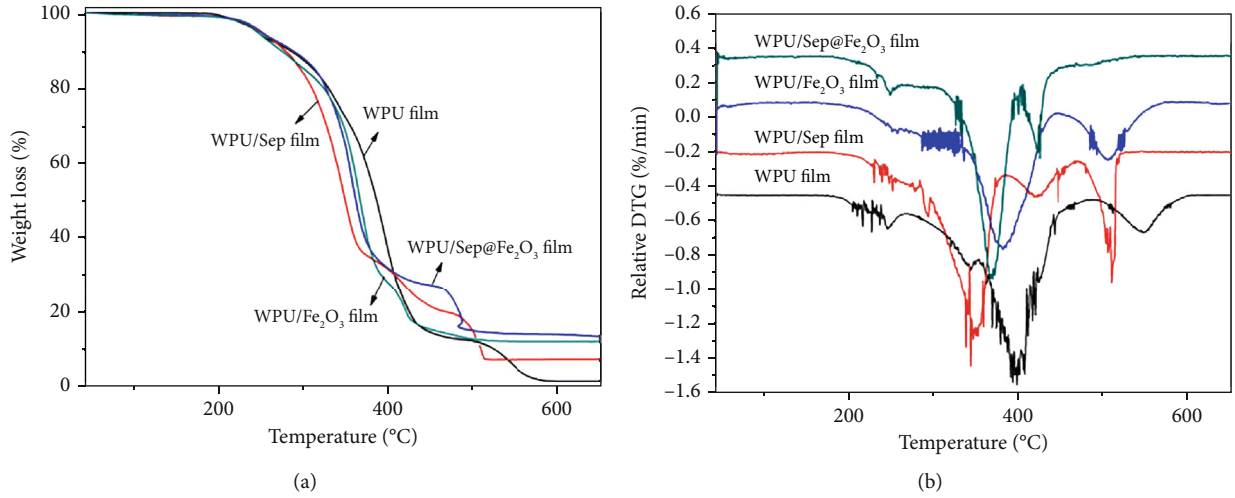

Figure 6: Thermal performance analysis of composite films: (a) TG and (b) DTG.

Table 2: Vertical combustibility data of cotton fabric coated with WPU composite films.

Samples	After-flame time (s)	After-glow time (s)
Cotton@S-1	14	31
Cotton@S-2	10	13
Cotton@S-3	10	34
Cotton@S-4	11	26

flame retardant. Therefore, Sep, Fe_2O_3, and Sep@Fe_2O_3 were used to prepare composites with WPU by LBL method. The TG and DTG thermograms of WPU and WPU composites were analyzed under air atmosphere shown in Figures 6(a) and 6(b). The first stage at 200-300°C involves the elimination reactions of H_2O, CO_2, and NH_3 and residual acetate groups because of partially hydrolyzing of WPU; the degradation step at 300-600°C is more complex and includes the further degradation of WPU residues to yield the carbon and hydrocarbons shown in Figure 6(a). The hydrocarbons in the TGA results have been discussed by our previous studies. The weight loss of WPU/Sep, WPU/Fe_2O_3, and WPU/Sep@Fe_2O_3 composites took place at 300-400°C and 400-600°C, for the loss of structure water of Sep and the thermal decomposition of WPU molecular. As is shown in Figure 6(a), at 600°C, the carbon residual percentages of WPU/Sep, WPU/Fe_2O_3, and WPU/Sep@Fe_2O_3 composites are 7.3%, 12.2%, and 13.4%, respectively, showing obvious difference from the control sample (1.4% for WPU). This increased percentage of char residue implies that Sep, Fe_2O_3, and Sep@Fe_2O_3 are favorable to improve the high-temperature resistance of WPU. Sep could act as the mass transport barrier to the volatiles produced during decomposition. Physi- and/or chemisorption occurring in the filler (Sep and Fe_2O_3)-matrix interphase may lead to the formation of physical network thereby enhancing the nanocomposite stability [7, 36].

The DTG (%/min) curves for thermal oxidation of the representative WPU and WPU composite samples are provided in Figure 6(b). Almost all the samples displayed two degradation peaks. It is noteworthy that the temperature at the greatest degradation peaks (T_{max}) decreased from

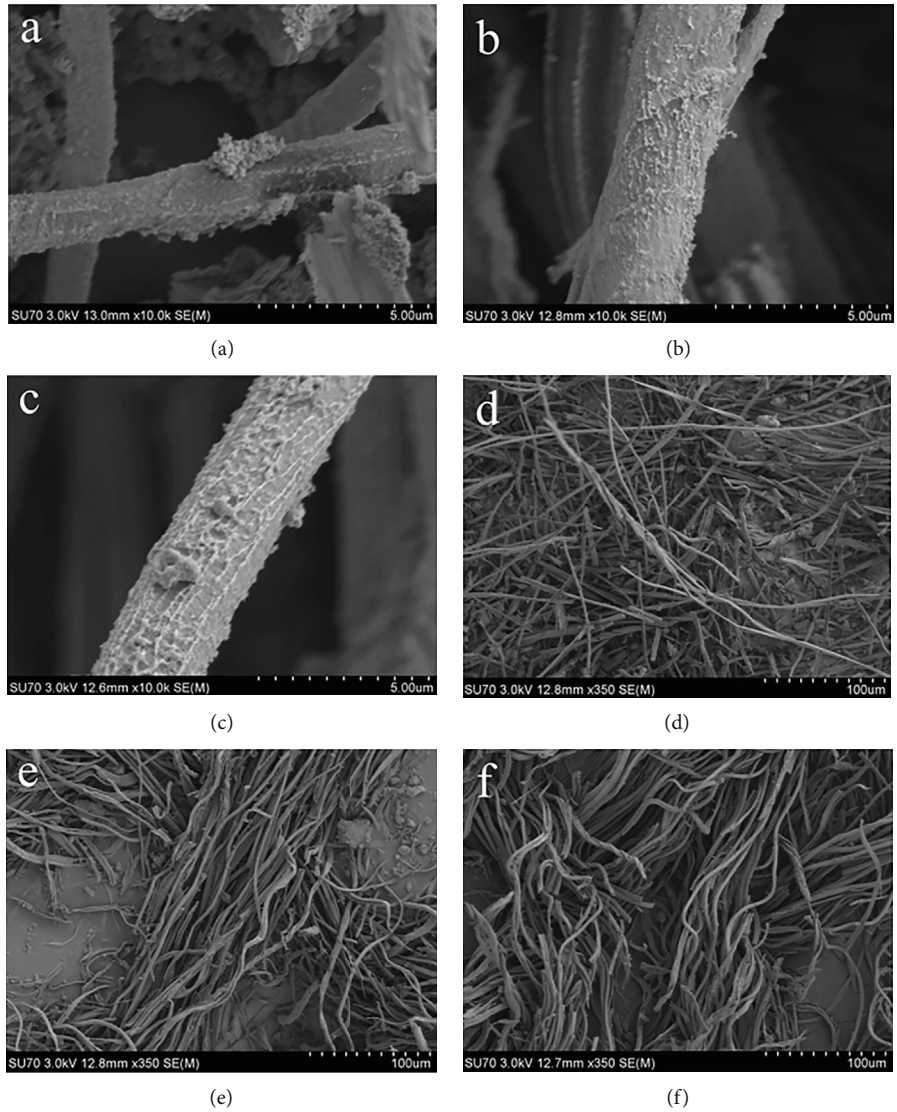

Figure 7: SEM images of carbon residues: (a, d) Cotton@S-2, (b, e) Cotton@S-3, and (c, f) Cotton@S-4.

397°C (for WPU) to 341°C, 378°C, and 366°C, for WPU/Sep, WPU/Fe_2O_3, and WPU/Sep@Fe_2O_3 composites, respectively. This decreasing of T_{max} is probably due to the catalytic carbonation of Sep and Fe_2O_3 in the WPU composites. This is generally attributed to a catalytic action played by the Lewis acidic sites of clays [37]; Fe_2O_3 itself is a kind of catalyst.

3.2.2. Flame-Retardant Properties of WPU Composites. For the catalytic carbon formation performance of Sep and Fe_2O_3, the flame-retardant property of WPU composites is improved. Considering that cotton fabric is a kind of flammable material and widely used in our daily life, a vertical flammability test was conducted on the coated cotton fabrics. Upon ignition, the noncoated cotton fabrics were burned for about 14 s and had nothing left. The burning time of cotton fabrics coated with WPU composite films is shown in Table 2. The coated cotton fabrics (coated with WPU/Sep film, WPU/Fe_2O_3 film, and WPU/Sep@Fe_2O_3 film) were burned just for 10 s and retained the original fiber structure of the textiles. Shown in Figure 7 are SEM images of cotton residues. From Figures 7(a)–7(c), we could see the integrity of cotton fiber coated with films, which are composed of carbon that converted from WPU films catalyzed by Sep or Fe_2O_3. Benefitting from the protection of WPU composite films, the cotton fabrics could keep their original structure. For these results, we could think that the WPU composite films have the potential to improve the flame-retardant property of cotton fabrics.

3.2.3. Combustion Behavior of WPU Composites. MCC is an effective approach for evaluating the combustion behavior of materials. The heat release rate (HRR) curves versus temperature of WPU and WPU composites are presented in Figure 8. For the WPU film, the thermal decomposition started at approximately 175°C and peaked (418.9 W/g) at 355.2°C. The decomposition of WPU ended at about 385°C. WPU composite films almost started to decompose

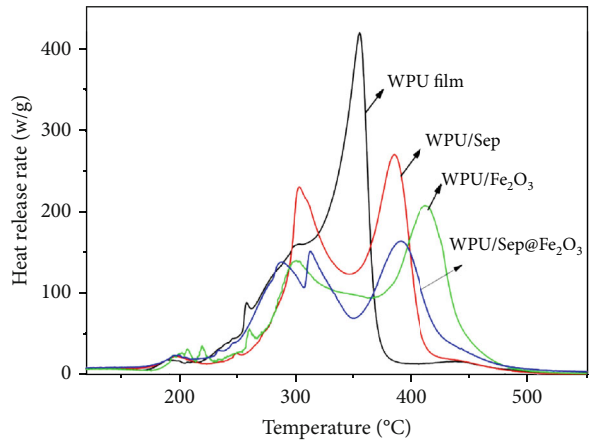

Figure 8: The heat release rate curves versus temperature of WPU and WPU composites.

Table 3: Microscale combustion data of the WPU and WPU composite samples.

Sample number	HRC (J/g-K)	PHRR (W/g)	Tp (°C)	THR (kJ/g)	Percentage of char (%)
S-1	470.0	418.9	355.2	27.0	3.1
S-2	302.0	269.9	385.0	26.0	6.9
S-3	231.0	206.9	412.2	26.3	7.6
S-4	184.0	164.2	390.6	25.2	14.3

Table 4: Mechanical properties of WPU composite membrane.

Samples	Breaking strength (N)	Break elongation (%)
S-1	3.2	353.2
S-2	2.7	69.6
S-3	7.0	425.8
S-4	4.9	17.1

at approximately 175°C and ended at approximately 485°C. In the presence of the flame-retardant system, the HRR peaked at 355.2°C for the WPU film (shown in Table 3). It increased by 30°C and decreased by 52°C to become two peaks at 385°C (269.9 W/g) and 303°C (241.9 W/g) for the WPU/Sep composite film. As is shown in Table 3, the total heat release (THR) of WPU decreased from 27 to 26 kJ/g whereas the percent char yield of WPU increased from 3.1 to 6.9% after being complexed with Sep. Moreover, the one peak in the HRR curve of the WPU split into two peaks after being complexed with Sep, and the HRR curve of the WPU/Sep composite film became broader with a less symmetric shape than that of WPU. When 6.7 wt.% Sep was replaced by 6.7 wt.% Fe_2O_3 or 6.7 wt.% Sep@Fe_2O_3, peak of heat release rate (pHRR) and THR decreased, and the temperature of heat release rate (T_{PHRR}) has little change. These results demonstrate the formation of a char layer over the surface of the material during the combustion process; the char layer could inhibit gaseous-fuel transport from the WPU to the flame front so as to reduce the HRR of the burning surface according to the combustion mechanism of clay-based composites during the MCC experiments. In addition, the char yield increased from 3.1% (for WPU) to 6.9%, 7.6%, and 14.3% for WPU/Sep, WPU/Fe_2O_3, and WPU/Sep@Fe_2O_3, respectively, indicating that the addition of inorganic materials could help the WPU to retain more degradation products in the condensed phase during combustion. The data suggested that the flame-retardant property of Sep@Fe_2O_3 is better than that of Sep or Fe_2O_3 alone. In addition, the results of MCC are coincident with the results of TG test (Figure 6(a)).

3.2.4. Tensile Properties. The mechanical properties of WPU and WPU composites are shown in Table 4. The increasing of breaking strength supports the strengthening of mechanical strength, and the decreasing of break elongation indicates the weakening of elasticity of WPU composites. The data presented in the table are the average of three readings. The breaking strength of S-2 decreased from 3.2 N to 2.7 N, as the result of stress concentration due to agglomeration of Sep microfibers. In the case of S-3, breaking strength increased from 3.2 N to 7.0 N, because the addition of Fe_2O_3 into the WPU matrix improved the interfacial adhesion among the WPU matrix through oxygen atoms (in Fe_2O_3 structure) and amino and hydroxyl groups (in WPU molecular structure), respectively [38, 39]. Considering Figure 4(e), the interface between Fe_2O_3 and WPU could not be observed, which means that the compatibility between those two materials is excellent. Therefore, the result of tensile properties of WPU composites is consistent with that of TEM. Sample S-4 was prepared by WPU and Sep@Fe_2O_3, which showed a significant improvement in mechanical property and small reduction in elasticity property. For oxygen atom and hydroxyl in Sep matrix and -NH-, C=O in WPU could form hydrogen bond formation to improve the mechanical strength of WPU composites. Meanwhile, interaction between WPU and inorganic materials could restrict the movement of polymer chains and reduce the elasticity property of WPU composites. In summary, the heat resistance and mechanical properties of WPU/Sep@Fe_2O_3 composites are confirmed in this work, proving that it has the potential to be used as a high temperature-resistant material.

4. Conclusion

In this work, Fe_2O_3 as a kind of flame retardant is loaded in Sep that was used for WPU. Flame-retardant properties of Sep, Fe_2O_3, and Sep@Fe_2O_3 were evaluated by VFT, TGA, and MCC measurements. The compounding of Sep@Fe_2O_3 with WPU could change the thermal stability of the material. Using VFT, it was found that the flame-retardant property achieved optimization when 6.7 wt.% Sep@Fe_2O_3 substituted 6.7 wt.% Sep or Fe_2O_3. In this case, the residual carbon percentages of WPU, WPU/Sep, WPU/Fe_2O_3, and WPU/Sep@Fe_2O_3 composites obtained from TG/DTG curves are 1.4%, 7.3%, 12.2%, and 13.4%, respectively. These results revealed that the thermal stability of WPU/Sep@Fe_2O_3 increased compared with that of WPU/Sep or WPU/Fe_2O_3. This phenomenon can also be observed in the MCC tests in terms of

HRC, PHRR, and THR. The values of char yield in TG and MCC tests were higher for samples treated with inorganic flame retardant than those that are untreated. These results show wonderful flame-retardant properties of Sep, Fe_2O_3, and Sep@Fe_2O_3 on WPU materials. Meanwhile, the mechanical property of WPU composites was improved. Therefore, the inorganic flame retardant could be used for preparing flame-retardant WPU composites with improved mechanical property.

Data Availability

The data is included in the manuscript already.

Conflicts of Interest

The authors declared that there are no conflicts of interest in this work. We declare that we do not have any commercial or associative interest that represents a conflict of interest in connection with the work submitted.

Acknowledgments

The present work is supported financially by the National Key R&D Program of China (No. 2018YFC1801500) and the Fundamental Research Funds for the Central Universities (No. 2232020G-04).

References

[1] H. Liang, L. Liu, J. Lu, M. Chen, and C. Zhang, "Castor oil-based cationic waterborne polyurethane dispersions: Storage stability, thermo-physical properties and antibacterial properties," *Industrial Crops and Products*, vol. 117, pp. 169–178, 2018.

[2] F. Naz, M. Zuber, K. Mehmood Zia et al., "Synthesis and characterization of chitosan-based waterborne polyurethane for textile finishes," *Carbohydrate polymers.*, vol. 200, pp. 54–62, 2018.

[3] R. Patel and P. Kapatel, "Waterborne polyurethanes: A three step synthetic approach towards environmental friendly flame retardant coatings," *Progress in Organic Coating*, vol. 125, pp. 186–194, 2018.

[4] D. K. Chattopadhyay and D. C. Webster, "Thermal stability and flame retardancy of polyurethanes," *Progress in Polymer Science*, vol. 34, no. 10, pp. 1068–1133, 2009.

[5] P. M. Visakh, A. O. Semkin, I. A. Rezaev, and A. V. Fateev, "Review on soft polyurethane flame retardant," *Construction and Building Materials*, vol. 227, pp. 116673–116679, 2019.

[6] H. X. Chen, H. Z. Lu, Y. Zhou, M. S. Zheng, C. M. Ke, and D. L. Zeng, "Study on thermal properties of polyurethane nanocomposites based on organo-sepiolite," *Polymer Degradation and Stability*, vol. 97, no. 3, pp. 242–247, 2012.

[7] H. X. Chen, M. S. Zheng, H. Y. Sun, and Q. M. Jia, "Characterization and properties of sepiolite/polyurethane nanocomposites," *Materials Science and Engineering A*, vol. 445-446, pp. 725–730, 2007.

[8] H. Y. Choi, C. Y. Bae, and B. K. Kim, "Nanoclay reinforced UV curable waterborne polyurethane hybrids," *Progress in Organic Coating*, vol. 68, no. 4, pp. 356–362, 2010.

[9] J. M. Yeh, C. T. Yao, C. F. Hsieh et al., "Preparation, characterization and electrochemical corrosion studies on environmentally friendly waterborne polyurethane/Na+-MMT clay nanocomposite coatings," *European Polymer Journal*, vol. 44, no. 10, pp. 3046–3056, 2008.

[10] B. K. Kim, J. W. Seo, and H. M. Jeong, "Morphology and properties of waterborne polyurethane/clay nanocomposites," *European Polymer Journal*, vol. 39, no. 1, pp. 85–91, 2003.

[11] S. Wang, X. Du, Y. Jiang et al., "Synergetic enhancement of mechanical and fire-resistance performance of waterborne polyurethane by introducing two kinds of phosphorus–nitrogen flame retardant," *Journal of Colloid and Interface Science*, vol. 537, pp. 197–205, 2019.

[12] F. Tabatabaee, M. Khorasani, M. Ebrahimi, A. González, L. Irusta, and H. Sardon, "Synthesis and comprehensive study on industrially relevant flame retardant waterborne polyurethanes based on phosphorus chemistry," *Progress in Organic Coating*, vol. 131, pp. 397–406, 2019.

[13] G. Wu, J. Li, and Y. Luo, "Flame retardancy and thermal degradation mechanism of a novel post-chain extension flame retardant waterborne polyurethane," *Polymer Degradation and Stability*, vol. 123, pp. 36–46, 2016.

[14] Y. Ren, Y. Dong, Y. Zhu, J. Xu, and Y. Yao, "Preparation, characterization, and properties of novel ultraviolet-curable and flame-retardant polyurethane acrylate," *Progress in Organic Coating*, vol. 129, pp. 309–317, 2019.

[15] H. Hu, Y. Yuan, and W. Shi, "Preparation of waterborne hyperbranched polyurethane acrylate/LDH nanocomposite," *Progress in Organic Coating*, vol. 75, no. 4, pp. 474–479, 2012.

[16] E. Boyles, H. Tan, Y. Wu et al., "Halogenated flame retardants in bobcats from the midwestern United States," *Environmental Pollution*, vol. 221, pp. 191–198, 2017.

[17] J. de Boer, P. G. Wester, H. J. C. Klamer, W. E. Lewis, and J. P. Boon, "Do flame retardants threaten ocean life?," *Nature*, vol. 394, no. 6688, pp. 28-29, 1998.

[18] L. S. Birnbaum and D. F. Staskal, "Brominated flame retardants: cause for concern?," *Health Perspectives*, vol. 112, no. 1, pp. 9–17, 2004.

[19] X. Chen, C. Ma, and C. Jiao, "Synergistic effects between iron-graphene and ammonium polyphosphate in flame-retardant thermoplastic polyurethane," *Journal of Thermal Analysis and Calorimetry*, vol. 126, no. 2, pp. 633–642, 2016.

[20] I. van der Veen and J. de Boer, "Phosphorus flame retardants: Properties, production, environmental occurrence, toxicity and analysis," *Chemosphere*, vol. 88, no. 10, pp. 1119–1153, 2012.

[21] Y. Lu, C. Wu, and S. Xu, "Mechanical, thermal and flame retardant properties of magnesium hydroxide filled poly(vinyl chloride) composites: The effect of filler shape," *Composites. Part A, Applied Science and Manufacturing*, vol. 113, pp. 1–11, 2018.

[22] V. Carretier, J. Delcroix, M. F. Pucci, P. Rublon, and J. M. Lopez-Cuesta, "Influence of Sepiolite and Lignin as Potential Synergists on Flame Retardant Systems in Polylactide (PLA) and Polyurethane Elastomer (PUE)," *Materials*, vol. 13, no. 11, pp. 2450–2471, 2020.

[23] Y. Pan, L. X. Liu, W. Cai, Y. Hu, S. D. Jiang, and H. T. Zhao, "Effect of layer-by-layer self-assembled sepiolite-based nanocoating on flame retardant and smoke suppressant properties of flexible polyurethane foam," *Applied Clay Science*, vol. 168, pp. 230–236, 2019.

[24] S. Pappalardo, P. Russo, D. Acierno, S. Rabe, and B. Schartel, "The synergistic effect of organically modified sepiolite in intumescent flame retardant polypropylene," *European Polymer Journal*, vol. 76, pp. 196–207, 2016.

[25] "Guillon," U.S. Patent 8, 629, 073B2, 2014.

[26] A. Gómez-Avilés, P. Aranda, and E. Ruiz-Hitzky, "Layered double hydroxide/sepiolite heterostructured materials," *Applied Clay Science*, vol. 130, pp. 83–92, 2016.

[27] Y. Chen, J. Dong, L. Qiu, J. K. Kim, F. Ding, and L. Zhou, "A catalytic etching-wetting-dewetting mechanism in the formation of hollow graphitic carbon fiber," *Chem*, vol. 2, pp. 299–310, 2017.

[28] D. H. Taffa, I. Hamm, C. Dunkel, I. Sinev, D. W. Bahnemann, and M. Wark, "Electrochemical deposition of Fe2O3in the presence of organic additives: a route to enhanced photoactivity," *RSC Advances*, vol. 5, no. 125, pp. 103512–103522, 2015.

[29] A. Biswas, I. S. Bayer, P. C. Karulkar, A. Tripathi, and D. K. Avasthi, "Vapor-phase deposition of regioregular and oriented poly(3-hexylthiophene) structures and novel nanostructured composites of interpenetrating poly(3-hexylthiophene) and polyaniline exhibiting full-color wavelength (400–1000nm) photoluminescence," *Journal of Applied Physics*, vol. 102, no. 8, pp. 083543–083548, 2007.

[30] S. Min, F. Wang, and Y. Han, "An investigation on synthesis and photocatalytic activity of polyaniline sensitized nanocrystalline TiO2 composites," *Journal of Materials Science*, vol. 42, no. 24, pp. 9966–9972, 2007.

[31] W. Feng, E. Sun, A. Fujii, H. Wu, K. Niihara, and K. Yoshino, "Synthesis and Characterization of Photoconducting Polyaniline-TiO2Nanocomposite," *Bulletin of the Chemical Society of Japan*, vol. 73, no. 11, pp. 2627–2633, 2000.

[32] J. W. Zhang, Y. Li, and S. Zhang, "Preparation, Characterization and Corrosion Evaluation of Poly(o-toluidine), Poly(m-Toluidine), and Poly(p-Toluidine) Blended with Waterborne Polyurethane," *Journal of Metals*, vol. 70, no. 11, pp. 2660–2666, 2018.

[33] C. H. Zhou, G. L. Li, X. Y. Zhuang et al., "Roles of texture and acidity of acid-activated sepiolite catalysts in gas-phase catalytic dehydration of glycerol to acrolein," *Molecular Catalysis*, vol. 434, pp. 219–231, 2017.

[34] A. Corma, J. Perez-Pariente, and J. Soria, "Physico-chemical characterization of Cu2+-exchanged sepiolite," *Clay Minerals*, vol. 20, no. 4, pp. 467–475, 1985.

[35] V. Li, "Acid–base behaviour and Cu2+ and Zn2+ complexation properties of the sepiolite/water interface," *Chemical Geology*, vol. 198, no. 3-4, pp. 213–222, 2003.

[36] F. Chivrac, E. Pollet, M. Schmutz, and L. Avérous, "Starch nano-biocomposites based on needle-like sepiolite clays," *Carbohydrate Polymers*, vol. 80, no. 1, pp. 145–153, 2010.

[37] F. Bellucci, G. Camino, A. Frache, and A. Sarra, "Catalytic charring–volatilization competition in organoclay nanocomposites," *Polymer Degradation and Stability*, vol. 92, no. 3, pp. 425–436, 2007.

[38] X. Zou, B. Sariyev, K. Chen et al., "Enhanced interfacial bonding strength between metal and polymer via synergistic effects of particle anchoring and chemical bonding," *Journal of Manufacturing Processes*, vol. 68, pp. 558–568, 2021.

[39] R. K. Naik, S. K. Panda, and V. Racherla, "A new method for joining metal and polymer sheets in sandwich panels for highly improved interface strength," *Composite Structures*, vol. 251, pp. 112661–112668, 2020.